

Removal of heavy metals lead and copper ions from waste water using green synthesized $\text{MnO}_2/\text{Mn}_2\text{O}_3$ nanoparticles

I. Aouadj ^a, H. Zerrouki ^a, L. Zenkhri ^a, M. S. Nedjimi ^{a,*}, M. L. Belfar ^a, S. Tlili ^b, K. Mokadem ^a

^a VPRS Laboratory, Faculty of Mathematics & Matter Sciences University of Kasdi Merbah, B.P. 511, 30000, Ouargla, Algeria.

^b LARENZA Laboratory, Kasdi Merbah Ouargla University, 30000, Ouargla, Algeria

The current study examined the removal of lead and copper ions from aqueous solutions using a variety of experimental techniques by producing manganese oxide sorbent nanoparticles ($\text{MnO}_2/\text{Mn}_2\text{O}_3$ -NPs) from a sunflower seed husk extract (*Helianthus annuus*). Key factors that affected the adsorption process were the pH level, contact time, starting metal ion concentration, and dose of the nanoadsorbent. Numerous analytical methods were employed to confirm the environmentally friendly manufacturing of $\text{MnO}_2/\text{Mn}_2\text{O}_3$ -NPs. According to the data, the $\text{MnO}_2/\text{Mn}_2\text{O}_3$ -NP had an average size of roughly 26.93 nm. The adsorption reaction rate was analyzed by comparing pseudo-first- and pseudo-second-rate models. According to the recorded data, lead and copper ions adsorption response on the $\text{MnO}_2/\text{Mn}_2\text{O}_3$ -NPs agreed on the paradigm of pseudo-second order. Langmuir and Freundlich's models assessed lead and copper sorption onto the absorbed substance. Considering the parameters that each model yields, the Langmuir isotherms emerge as the favoured choice for the adsorption of Pb^{2+} and Cu^{2+} ions on $\text{MnO}_2/\text{Mn}_2\text{O}_3$ nanoparticles. $\text{MnO}_2/\text{Mn}_2\text{O}_3$ -NPs show promise as an adsorbent material to remove heavy metals from water solutions.

(Received January 1, 2025; Accepted April 3, 2025)

Keywords: Manganese oxide nanoparticles, Green synthesis, Adsorption, Heavy metals, Kinetics model, Isotherm model

1. Introduction

All living beings' ability to survive and the advancement of humankind depends on water, One of the most important natural resources in the world. The issue of water shortage has grown to be a significant barrier to economic growth as industrialization and urbanization have accelerated and Water consumption is rising quickly. Meanwhile, water pollution has grown to be a major worldwide environmental concern, particularly the presence of toxic metals including Pb, Cd, Cu, and Hg in water. Metallurgy, mining, electroplating, chemical plants, residential wastewater, and agriculture are the principal sources of heavy metals discharged into the water. Because heavy metals can accumulate naturally in the food chain, they could pose a significant risk to human health [1]. For instance, exposure to heavy metals may harm the kidneys, lungs, central and mental nervous systems, and other organs[2, 3].

Furthermore, because heavy metals cannot be broken down by microbes after they are released into the environment and instead accumulate along the food chain, they can have a negative impact on the ecosystem and other ecological receptors. The majority of heavy metals have even been shown to be carcinogenic[4], making them extremely poisonous[5]. Therefore, eliminating these hazardous metal ions from wastewater is turning into a major concern. Many conventional techniques, encompassing chemical precipitation [6], reverse osmosis [7], electrochemical treatment methods [8], ion exchange [9], membrane filtration [10], coagulation[11], extraction [12], irradiation [13], and adsorption[14], could be utilized to

* Corresponding author: nedjimi2011@gmail.com
<https://doi.org/10.15251/DJNB.2025.202.395>

eliminate toxic metals ions[15]. But the last technique is the best one due to cost-effective, highly efficient, and easily operated method of eliminating traces of heavy metal ions[16].

A lot of research has been done on adsorbent manufacturing, including zeolites, polymer compounds, activated carbons, biofuels, and industrial by products[17, 18]. However, these adsorbents have significant drawbacks, including low economic viability, limited loading capacities, insufficient of sites for metal-ion binding, and inadequate selectivity. In light of these challenges, researchers have focused on creating nano-adsorbents (metal oxides)to remove pollutants from wastewater[19].Selenium, silicon oxide, titanium, manganese, aluminum, iron, and zinc oxide nanoparticles are among the metal oxides that have been produced as nano-adsorbents [20]. Due to their size, vast surface area, changing oxidation states, electrical and magnetic characteristics, eco-friendliness, and high adsorption effectiveness [21, 22].

Multiple kinds of manganese oxides (MnO , MnO_2 , Mn_2O_3 , and Mn_3O_4) are One of these oxide NPs, which are intriguing families of inorganic materials because of their cost-effectiveness, wide range of oxidation states, and diverse [23].Manganese oxide nanoparticles have excellent physico-chemical characteristics that can be used in across a range of fields , including water treatment [24]. Numerous techniques, including the sol-gel method [25], hydrothermal method [26], photochemical method [27], wet chemical method[28] and pyrolysis method [21] have been used to produce manganese oxide nanoparticles. There was also the green synthesis method for producing this nanoparticles. This approach of creating nanoparticles was economical, efficient, and good to the environment. It employs microorganisms as raw materials, including plant extract, biopolymer-alginate, and bacteria or fungi [29].

In this study, a novel precursor, from *Helianthus annuus* (sunflower) seed husk extract, an agricultural waste, is used to facilitate the green synthesis of MnO_2/Mn_2O_3 NPs using the sol-gel method. The nanoparticles synthesis is mostly carried out by phytochemicals found in the using plant extract. The generated nanoparticles were characterized using energy-dispersive spectroscopy (EDS), Fourier transform infrared (FT-IR) spectroscopy, field-emission scanning electron microscopy (SEM), UV-Vis spectroscopy, and X-ray diffraction (XRD). Additionally, we assessed the many factors affecting the adsorption process, including the initial metal content, contact duration, pH of the solution, and adsorbent dosage. Moreover, kinetic and equilibrium research on the metal ion adsorption onto MnO_2 - Mn_2O_3 -NPs.

2. Experimental

2.1. Materials

Manganese nitrate tetra hydrate ($Mn(NO_3)_2 \cdot 4H_2O$),Copper(II) nitrate trihydrate($Cu(NO_3)_2 \cdot 3 H_2O$),Lead nitrate ($Pb(NO_3)_2$) were purchased from Merck chemicals was purchased from Merck chemicals, double distilled water. Sun flower seeds husks (*Helianthus annuus* seeds shells) were obtained from local market, Ourgla, Algeria.

2.2. Extract preparation

Following cleaning, the white husks of sunflower seeds were dried overnight at $60^\circ C$ in an oven before being ground into a powder. The extract was made ready by adding 9.2 g of SFSH powder in 100 ml DD Water, boiling, and stirring at $70^\circ C$ for 30 min. The brown obtained extract was first exhaustively filtered with Whatman filter paper N°2 then kept for later use at $4^\circ C$.

2.3. Green synthesis of MnO_2/Mn_2O_3 -NPs using sunflower seeds husks

10ml of SSHE was putted in 50 ml beaker.2 g of manganese nitrate was reduced in the extract, then the mixture was heated at $70^\circ C$ for 3h and 30 min under constant stirring, at the end of reaction showed a black gel formed at bottom of beaker. The obtained gel was transformed placed in a ceramic crucible and heated to $400^\circ C$ for two hours in a muffle furnace (Nabertherm GmbH, Germany). Finally, obtained a black powder. The schematic of the green synthesis of our nanoparticle is shown in figure1.

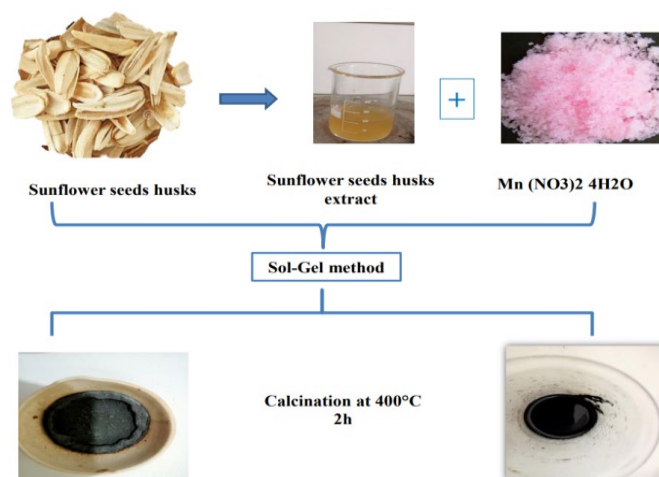


Fig. 1. Green synthesis of MnO_2/Mn_2O_3 nanoparticles.

2.4. Characterization techniques

Several methods were used to characterize the MnO_2/Mn_2O_3 nanoparticles, including UV–visible, FTIR, DRX, BET, SEM and EDX. The optical properties were determined by UV –visible spectrophotometer (Cary 100 Agilent technology) from 250–800nm wavelengths. The functional group of MnO_2/Mn_2O_3 -NPs was recording by Fourier transform infrared (FTIR) spectrophotometer (Cary 8000 Agilent technology) from 400–4000 cm^{-1} . The particles' size and crystalline structure were investigated using X-ray diffraction (XRD, Proto) with CuK α radiation (1.5406 Å) at diffraction angles (2θ) ranging from 30° to 80°. A Brunauer-Emmett-Teller surface area analyzer was used to measure the surface area, pore volume, and pore size distribution. The structure of shapes and elements composed in the sample were analysed by Scanning electron microscope (SEM) and Energy dispersion spectroscopy (EDX, Zeiss) respectively. Finally, concentration of metal ions (Pb^{2+} and Cu^{2+}) in an aqueous solution was employed (Analytic Jena Contra 800 Atomic Absorption Spectrometer, Germany).

2.5. Batch investigation of adsorption

Adsorption tests were carried out at room temperature ($25 \pm 1^\circ C$) with Pb, and Cu ions as the adsorbate and MnO_2/Mn_2O_3 NPs as the adsorbent. By dissolving an appropriate amount of copper (II) and lead nitrate in deionized water, for preparing a stock solution containing each one metal. Experiments of batching adsorption were conducted using a variety of parameters, including pH (which ranges from 2 to 8), starting metal ion concentrations (5 to 25 $mg L^{-1}$), contact times (10 to 60 minutes), and adsorbent doses (10 mg to 100 mg).

Each experiment involved sharking 25 mL of solutions with varying concentrations of each metal ion at 200 rpm and 25°C. The solution was filtered with Whatman100 filter paper. An atomic absorption spectrophotometer (AAS) was used to measure the concentration of each metal ion in the filtrate. The adsorption capacity ($mg g^{-1}$) and adsorption efficiency (%) of MnO_2/Mn_2O_3 -NPs were determined using equations (1) and (2).

$$q_e = \frac{C_i - C_e}{w} \times V \quad (1)$$

$$P(\%) = \frac{(C_i - C_e)}{C_i} \times 100 \quad (2)$$

C_i and C_e represent the initial and equilibrium concentrations of metal ions in the solution ($mg L^{-1}$), respectively. V is the solution's volume(L), and W is the nano sorbent's weight (g).

2.6. Adsorption models kinetics description

The pseudo-first-order dynamics model states that adsorption only takes place at discrete sites and the adsorbed ions do not interact with one another. On the other hand, the number of accessible spaces affects the absorption frequency according to equation (3), The following is his model of the kinetic process[30]:

$$\ln(q_e - q_t) = q_e - k_1 t \quad (3)$$

In 1999, Ho and Mckay described the pseudo-second-order template for the kinetics of $[M^{2+}]$ adsorption on a sorbent for the first time. [30].This model predicts behaviour over the whole adsorption range on assuming that the step that determines the rate is chemical adsorption. Here, the adsorption capacity determines the adsorption rate [31]. Equation (4) provides the pseudo-second-order equation[32].

$$\frac{t}{q_t} = \frac{t}{q_e} + \frac{1}{K_2 q_e^2} \quad (4)$$

2.7. The isotherms of the adsorption models

Adsorption isotherms offer crucial physicochemical data that can be used to demonstrate the adsorption process' suitability as a standalone procedure. We examined the Langmuir and Freundlich models. The Freundlich model deals with heterogeneous adsorption, while the Langmuir model focuses with monolayer adsorption with a constant adsorption energy.[33].Table1 (equation (5)and 6)) contains the following parameter definitions: Q_{max} denotes the maximum adsorption capacity of monolayer sorption, whereas q_e denotes the adsorption capacity at equilibrium in ($mg\ g^{-1}$). C_e is the ion concentration at equilibrium in (mg/L); K_f is the adsorption capacity on the solid adsorbent; n is the adsorption intensity on the adsorbent surface; and K_L is the Langmuir equilibrium constant, which indicates the adsorption strength in ($L\ mg^{-1}$).[34, 35].The Langmuir isotherm constant, which can be connected in equation (7), can be used to determine the fundamental properties of the Langmuir isotherms.

$$R_L = \frac{1}{1 + K_L C_i} \quad (7)$$

Table 1. Formulas for isotherm models.

Isotherm Model	Adsorption Equation	Equations
Langmuir	$\frac{C_e}{q_e} = \frac{1}{K_L q_{max}} + \frac{C_e}{q_{max}}$	(5)
Freundlich	$\log q_e = \log K_f + \frac{1}{n} \log C_e$	(6)

3. Results and discussion

3.1. Crystal shape and crystallite size

The XRD diffraction patterns of the green synthesis of MnO_2/Mn_2O_3 nanoparticles that annealed at $400^\circ C$ displayed in Figure 2. The diffractogram confirmed the existence of two crystalline phases MnO_2 and Mn_2O_3 . The peaks position at (2θ) values of $37.70^\circ, 41.09^\circ, 43.18^\circ, 59.60^\circ, 65.48^\circ$ and 72.86° corresponding to crystalline planes of (011), (020), (111), (222), (002) and (112) which confirmed the formation of the Orthorhombic crystal phase for MnO_2 (JCPDS card N° 00-050-0866) [36].

The other peak position with 2θ values of $33.39^\circ, 38.67^\circ, 45.65^\circ, 49.72^\circ, 55.64^\circ, 57.04^\circ, 66.19^\circ$ are attributed to the crystal planes of (222), (400), (332), (431), (440), (433), (622) which relate to the Cubic crystal system of Mn_2O_3 (JCPDS card N°00-001-1061) [37].The Scherrer

equation (8) was utilized to determine the average crystallite size (nm) of the synthesized nanoparticle.

$$D = K\lambda / \beta \cos\theta \quad (8)$$

where θ is the Bragg angle of diffraction, D is the crystalline size (nm), λ is the x-ray wavelength (1.5406 \AA), and FWHM is the full width at half maximum of the most intense diffraction peak[38]. The computed average size of $\text{MnO}_2/\text{Mn}_2\text{O}_3$ NPs was 26.93 nm.

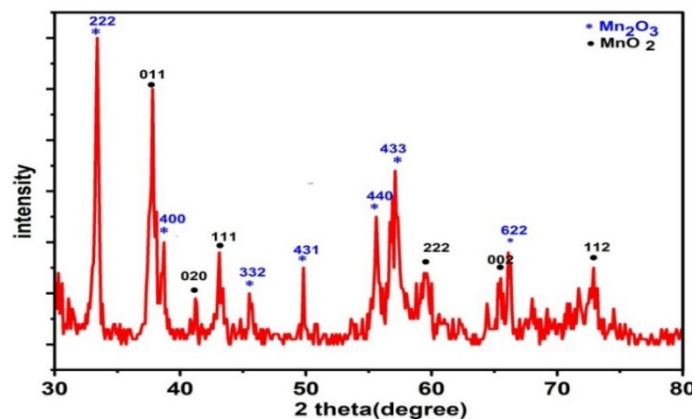


Fig. 2. XRD diffraction patterns of GS- $\text{Mn}_2\text{O}_3/\text{MnO}_2$ NPs calcinated at $400 \text{ }^\circ\text{C}$.

3.2. Morphology and particle size

SEM was used to analyse the morphology of the green-synthesized $\text{MnO}_2/\text{Mn}_2\text{O}_3$ nanoparticles.

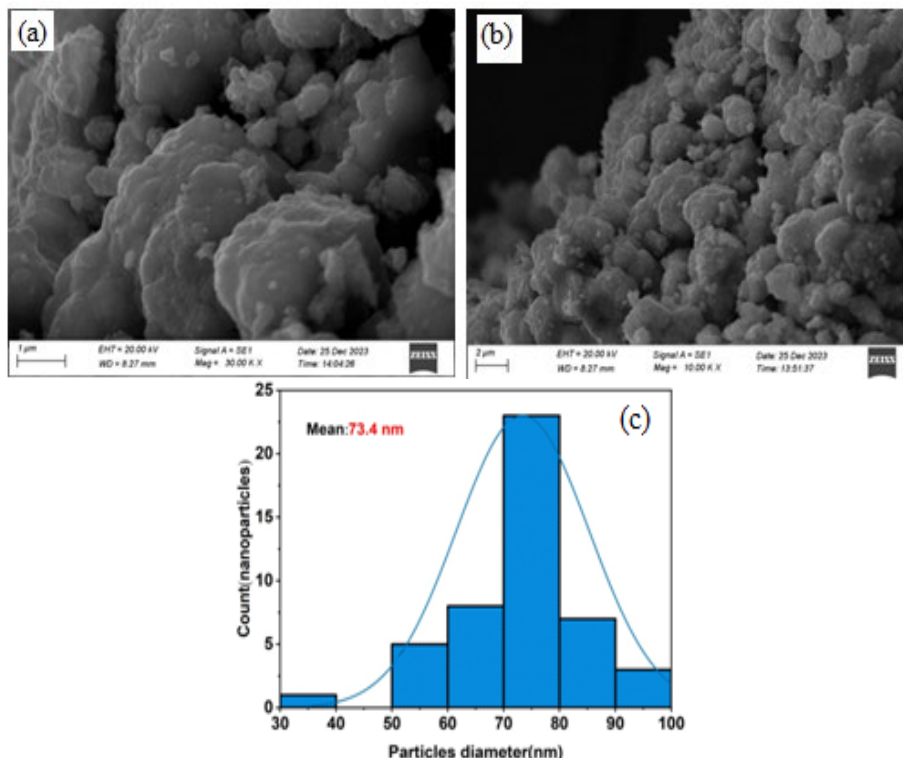


Fig. 3. (a, b) SEM image of GS- $\text{MnO}_2/\text{Mn}_2\text{O}_3$ - NPs and (C) their particle size distribution.

Figure 3 a, b shows a particle's spherical topology with agglomeration. According to SEM analysis, it was discovered that the nanoparticles ranged in size from 30 to 100 nm, with an average of 73.4 nm (figure 3C). The process of synthesized nanoparticles growing larger is caused by their aggregation and agglomeration, which is attributed to their greater surface area and density[39]. In addition, the EDX results (figure4) showed that the sample included Mn and O. The presence of varying percentages of Mn and O in the nanoparticle sample was validated by the EDX chemical composition analysis (table 2). elemental weight percentages of Mn and O were found to be greater, at 63.82% and 36.18%, respectively. The data show that most of the particles that develop are specific to MnO₂ NPs.

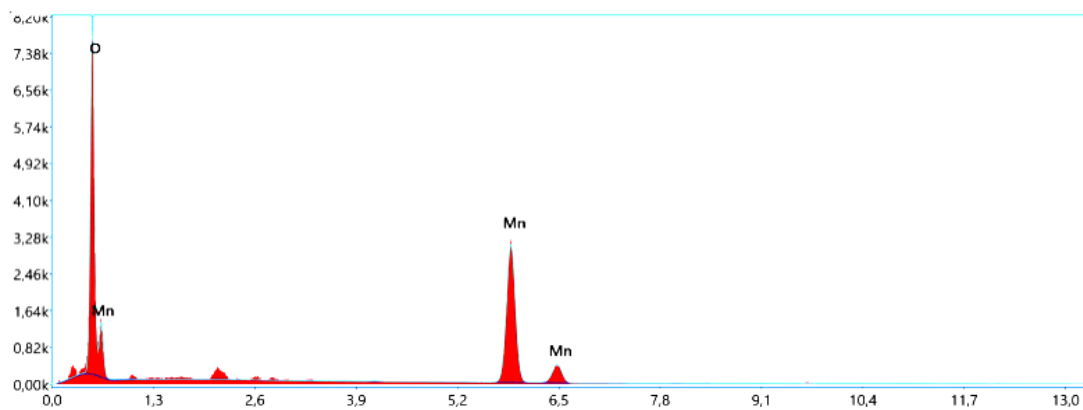


Fig. 4. EDX spectrum of GS- MnO₂/Mn₂O₃ NPs at 400 °C.

Table 2. Elemental Composition of synthesized nanoparticle.

Element	Weight%	Atomic%
O	36.18	66.06
Mn	63.82	33.94
Total	100	100

3.3. BET analysis

The most popular technique for figuring out a solid material's surface area is the Brunauer-Emmett Teller method. Physical adsorption of a gas into a solid surface and the determination of the quantity of adsorbate gas that forms a monomolecular layer on the surface yield a powder's specific surface area. Findings showed that synthetic MnO₂/Mn₂O₃ NPs would be useful for action to treat lead and cooper-contaminated l wastewater because of their surface area of 62,99 m² g⁻¹, 16,12 nm pore size, and 0,18 cm³ g⁻¹ pore volume. Figure 5 displays the produced adsorption-desorption isotherms curve for the nanoparticle.

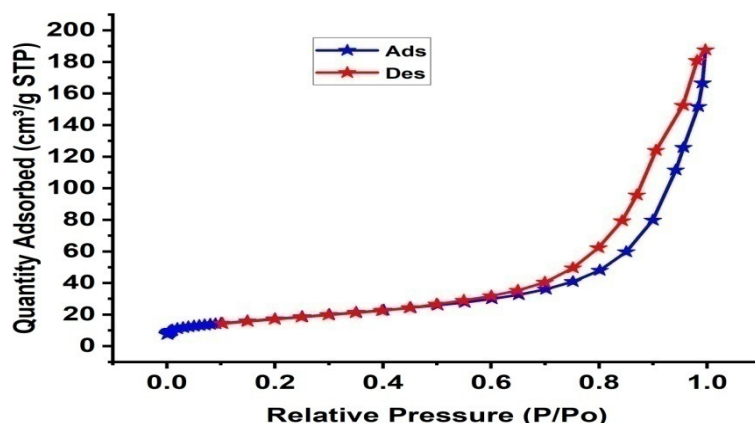


Fig. 5. Adsorption- desorption isotherms curve of the MnO_2/Mn_2O_3 nanoparticle.

3.4. FT-IR studies

The FTIR spectrum of the synthesized nanoparticles after annealing at $400^\circ C$ is displayed in figure 6, which appeared several absorption peaks. The stretching and bending vibration of the C–H bond was determined to be the source of the absorption peak at about 2102 cm^{-1} . [40]. The broad band at 1736 cm^{-1} could have been linked to the carbonyl group (C=O). The other peaks, which occurred at 1369 and 1222 cm^{-1} were ascribed to the vibration. vibration of the –CN bond and carboxylic groups, accordingly [41]. Yet, the peaks that emerge at $454, 551$ and 656 cm^{-1} may be assigned to Mn–O and Mn–O–Mn [42, 43]. That prove the formation of MnO_2/Mn_2O_3 NPs.

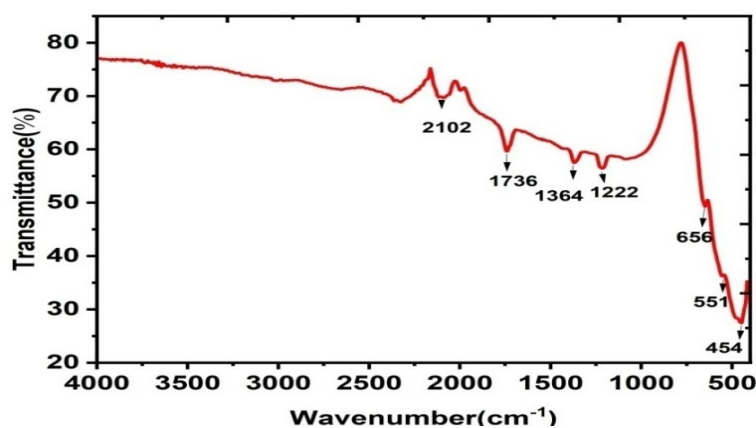


Fig. 6. FT-IR spectrum of MnO_2/Mn_2O_3 NPs annealed at $400^\circ C$.

3.5. UV–vis studies

The optical characteristics of the generated MnO_2/Mn_2O_3 nanoparticles were investigated in the $250\text{--}800\text{ nm}$ wavelength range using a UV-visible spectrophotometer. A wide absorption peak at 293 nm wavelength was found in figure 7a, suggesting the possibility of the formation of MnO_2/Mn_2O_3 nanoparticles. About terms the optical band gap energy utilising Tauc's relation (equation (9)) [44].

$$(ah\nu)^n = A (h\nu - E_g) \quad (9)$$

where $h\nu$ is the photon's energy and α is the absorption coefficient. $n = 2$ for a direct transition, whereas A is the standard.

The optical band gap energy (E_g , eV) of green synthesis MnO_2/Mn_2O_3 NPs using sunflower seeds husks was obtained at 4.86 eV (figure 7b). It has a higher value with direct band gap [45, 46]. The rise is cause a decrease in nanoparticle particle size, Thus a tiny particle size contributes to enhanced electrochemical performance, reduced energy conversion device costs, and improved electrochemical characteristics for successful remediation applications[23, 47].

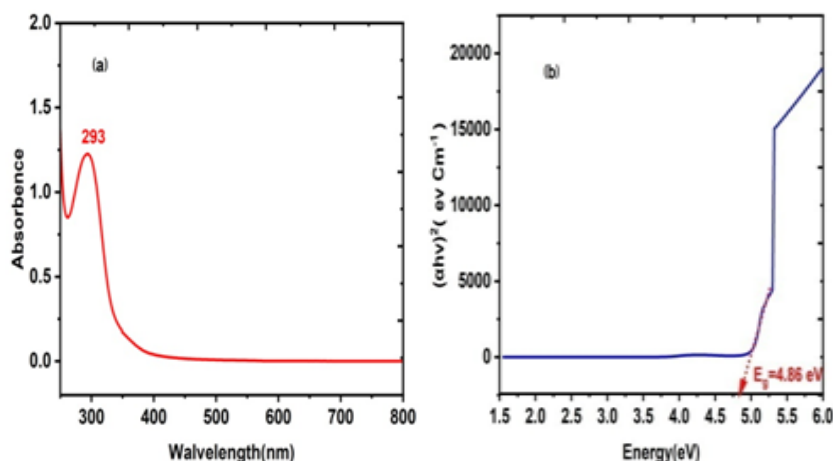


Fig. 7. (a) UV-Visible spectrum of synthesised MnO_2/Mn_2O_3 NPs, (b) direct bandgap transition using Tauc's method.

3.6. Sorption studies

3.6.1. Effect of pH

One of the most important variables in the metal ion adsorption process onto an adsorbent is pH. The worth's of MnO_2/Mn_2O_3 nanoparticles' sorption capacities for Pb(II) and Cu(II) at various pH solutions (2, ... 8), 20 mg L^{-1} of initial concentration and 20 mg adsorbent, are evident in (figure 8a). According to the findings, sorption capacity values rise with increasing pH. At alkaline conditions (pH 8). The elimination of lead and copper was found to be 97.51% and 99.90%, respectively. At acidic (pH 5), lead was found to be 42% while (pH 2) copper to be 62.42%.

The nano-sorbent exhibits an increase in sorption capacity values when pH rises, due to an increased net attractive force that may lead to deprotonation to the most active [48]. As such, decreased metal sorption capacity was seen at lower pH values, which may be connected to the hydronium ions and metals competitive adsorption. Furthermore, fewer metal ion binding sites are present on the surfaces of nano sorbents due to a larger concentration of hydronium ions, creating the appearance that the surfaces have a positive electrical charge [49].

3.6.2 Effect of sorbent dosage

In the present research, the sorbent of MnO_2/Mn_2O_3 nanoparticles were varied from 10 to 100 mg at pH 7, starting concentration 20 mg L^{-1} , and the contact time was 30 min for every kind of metal ion. As demonstrated in figure 8b, an increase in the dose of MnO_2/Mn_2O_3 -NPs from 10–20 mg resulted in a confirmed increase in lead removal efficiency (79.83%). As the dosage was increased from 10 to 100 mg, the copper elimination efficiency rose from 97.48% to 99.86%.

Generally, the elimination effectiveness of metal ions tends to rise as the amount of adsorbent is increased due to greater numbers of surfaces and binding sites available. Yet, elimination effectiveness loses some of its original efficiency after a particular dosage [50, 51]. When the amount of MnO_2/Mn_2O_3 nanoparticles increased, the amount of adsorption decreased. According to one theory was that, in the early stages when there was a big quantitative amount of heavy metals, the adsorption process was sped up by increasing the dosage of nanosorbent before it reached its maximum, or saturation, so creating additional adsorption sites. However, because the identical cations were dispersed across a larger surface area, the heavy metal that remained in

solutions could not adsorb on the accessible adsorption sites of additional nanoparticles after the adsorption reached equilibrium [52].

3.6.3. Effect of stirring time

At pH 7, the effects of shaking time were examined using a starting concentration of 20 mg L⁻¹ and 20 mg of nanosorbent. Figure 8C displays the findings of elimination for Pb(II), and Cu(II) from wastewater at various shaking durations ranging from 10 to 60 minutes. According to the results, Pb(II) was removed with an effective removal rate of 77.95% after 50 minutes and Cu(II) at 99.69% during 60 minutes. Also shown in the graph Pb(II) adsorption started quite quickly and then slowed down after 10 minutes, It is most likely due to M²⁺ migrating from the outermost layer into the micropores due to the growing occupancy of the active regions that is causing this little downward trend after 10 minutes [28]. Regarding the elimination of Cu(II) ions, it has been noted that removal effectiveness increases with longer contact times. It could be explained by an increase in the length of the interaction between the active sites on the nanoadsorbent and metal ions. Additionally, removability efficiency grows slowly in the later stages after being rapid in the first. This is mostly because there are initially larger vacant places on the adsorbent surface, although they eventually become less over time [25, 53].

3.6.4. Initial concentration

The adsorption of copper and lead metal ions from wastewater onto MnO₂/Mn₂O₃ nanoparticles is shown in Figure 8d. which were examined With different starting levels (5, 10, 15, 20, and 25 mg L⁻¹) under ideal conditions for each metal ion. The study of metal ions' adsorption at various concentrations demonstrates that the clearance percentage drops as the metal ion concentration rises. Under a starting concentration, the highest elimination capacities of Pb(II), and Cu(II) were 94.03%, and 99.95%, respectively.

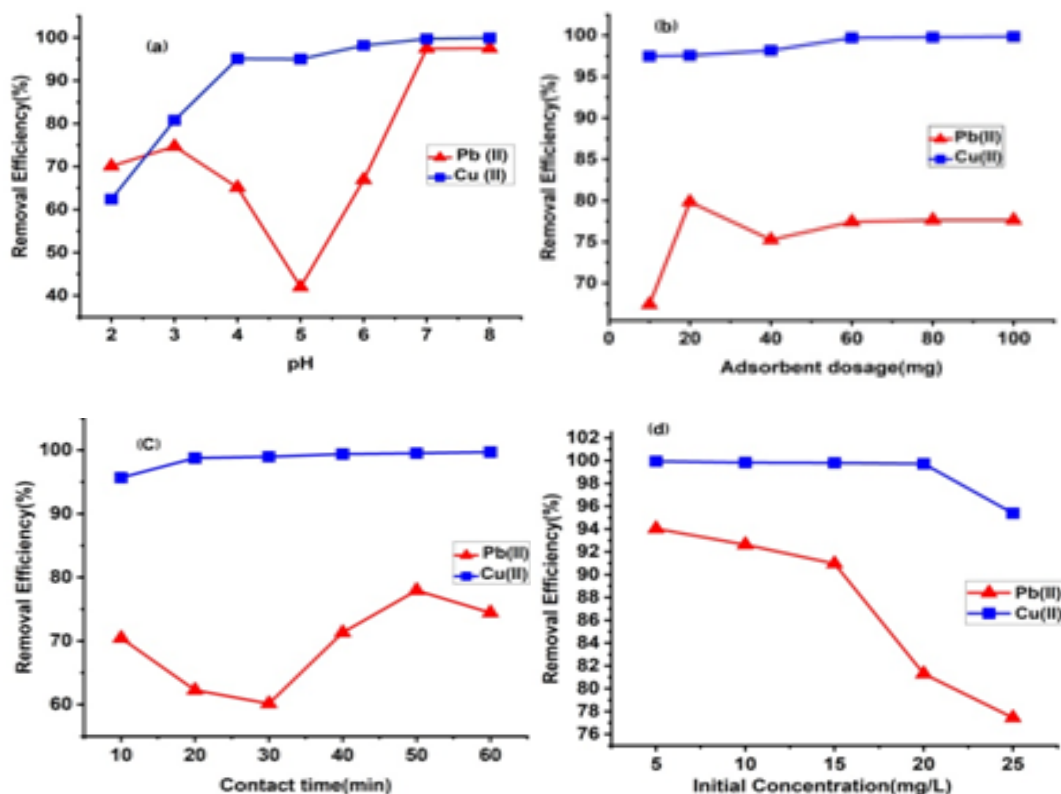


Fig. 8. Variability in MnO₂/Mn₂O₃-NPs removal effectiveness of Pb(II) and Cu(II) under various experimental settings.

This phenomenon demonstrates that the concentration of the metal and the adsorption efficiency are strongly related. Because there are more absorbable vacant sites available, at low metal concentrations, the frequency of metal ions on the nanosorbent rises. While the higher concentrations of metal ions result in fewer accessible adsorption sites, which lowers the rate at which these ions are removed [26, 27].

3.7. Adsorption isotherms

Freundlich and Langmuir were employed to identify the experimental data's homogeneous and heterogeneous characteristics. Figure 9 and Table 3 display the values derived from these models for the various parameters. The highest adsorption capacity, or q_{max} , was determined to be 2000 mg adsorbed per gram of MnO_2/Mn_2O_3 nanoparticles for copper and 26.44 mg for lead.

The isotherm is considered favorable if the Langmuir isotherm constant (R_L) is between zero and one; irreversible if R_L equals zero, linear if R_L equals one, and unfavorable if R_L exceeds one. All starting amounts of lead and copper showed good adsorption, with the computed value of R_L falling between 0.04 and 0.76, respectively. A suitable condition for Freundlich adsorption isotherms is demonstrated by an adsorption intensity (n) of the MnO_2/Mn_2O_3 nanoparticles that is calculated to be between 1 and 10. The values for lead and copper adsorption were determined to be 2.20 and 4.03, respectively, suggesting that the conditions for Freundlich adsorption isotherms were favorable. In removing lead and copper by MnO_2/Mn_2O_3 nanoparticles (figure 9 a,b,c,d), high R^2 values demonstrate how the experimental findings matched the Langmuir model more than the Freundlich model, suggesting a monolayer rather than a heterolayer adsorption behavior.

According to this model, adsorption forces are similar to those resulting from chemical interactions. Consequently, the adsorption energy is constant across the surface and there is no adsorbate trans-migration on the surface plane. Additionally, once a molecule has established itself at a certain location, no further adsorption is feasible [54].

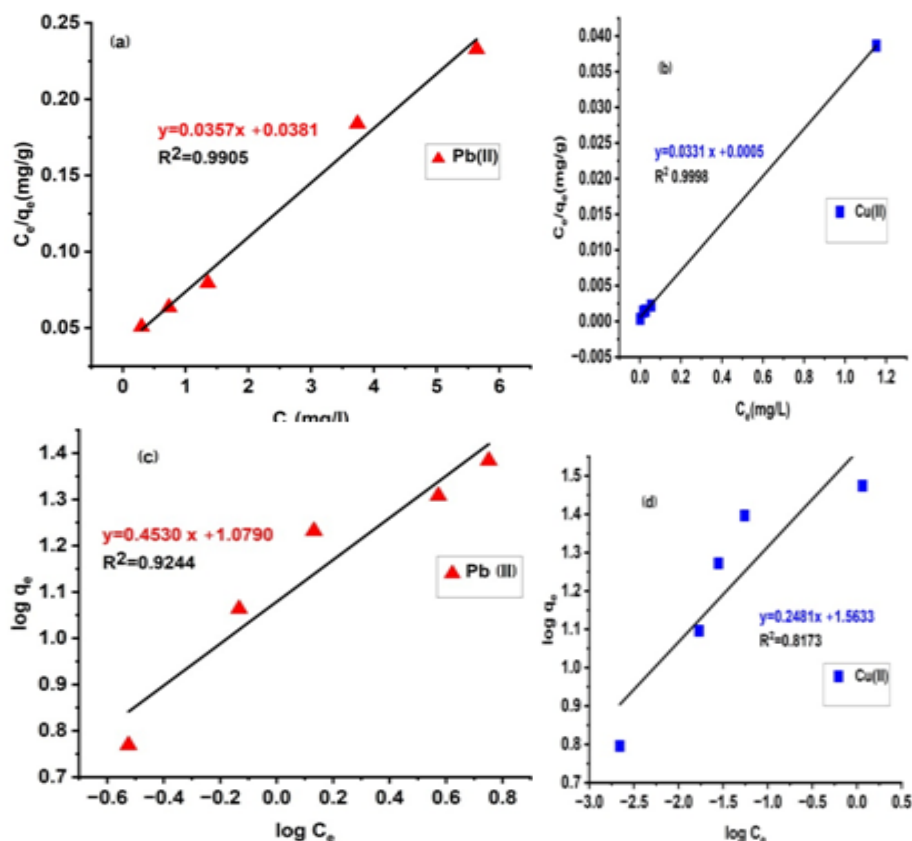


Fig. 9. (a,b) Langmuir graphs and (c,d) Freundlich diagram for the adsorption process of Pb(II), and Cu(II) through MnO_2/Mn_2O_3 NPs at interaction period: 30 min, amount dosage: 0.02 g and pH: 7.

Table 3. Parameters of Isotherm models.

Equilibrium Models	Parameters	Pb ²⁺	Cu ²⁺
Langmuir	q _{max} (mg g ⁻¹)	26.24	2000
	K _L (L mg ⁻¹)	1.06	0.015
	R _L	0.04	0.76
	R ²	0.9905	0.9998
Freundlich	K _f (mg g ⁻¹)	11.99	36.58
	1/n	0.45	0.24
	n	2.20	4.03
	R ²	0.9244	0.8173

3.8. Adsorption kinetics models

The selected nanoparticles' adsorption kinetics had to be evaluated. Accordingly, the most crucial elements influencing the sorbents' adsorption efficiency are their quick absorption, high q_e , and brief contact duration. Based on the kinetic investigations, the best shaking times for removing Pb²⁺ and Cu²⁺ were 50 and 60 minutes, respectively. The M²⁺. Equations (3) and (4) demonstrate how the Lagrange equation was used to characterize the M²⁺ adsorption kinetics as pseudo-first-order or pseudo-second-order kinetics, respectively. Here, k_1 (min⁻¹) represents the constant rate for the -firte-order template, q_t represents the adsorbate concentration at time t , q_e represents the adsorbate concentration at equilibrium, and k_2 (g.mg⁻¹.min⁻¹) represents the rate constant for the ps-sec-order model. There was a considerable difference between the value predicted by the ps-first-order equation and the actual value of q_e (table 4). Consequently, this theory was categorically rejected due to the extent of M²⁺ adsorption on the MnO₂/Mn₂O₃ -NPs. Nevertheless, when the pseudo-second-order rate model was applied, a linear relationship with a high R² was found (Figure 10). According to the data, the expected q_e value of the second-order rate model equation was rather similar to the actual q_e value (table 4). All of these outcomes confirmed that the pseudo-second-order kinetic template's predictions were met by the adsorption process. As is well known, the pseudo-second-order suggested a chemisorption process involving both ion exchange and covalent forces[55].

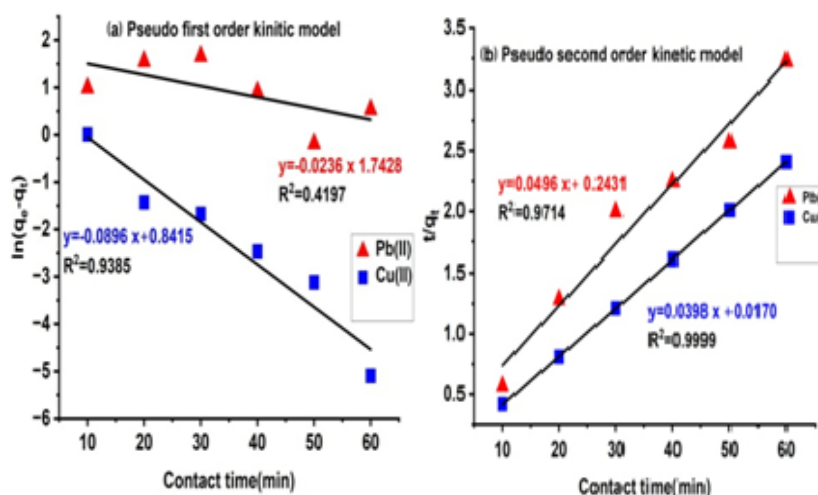


Fig. 10. (a) Pseudo-first order, (b) Pseudo-second order models for the adsorption metal ions using MnO₂/Mn₂O₃- NPs at initial concentration: 20 mg L⁻¹, dose: 0.02 g, and pH:7.

Table 4. Adsorption kinetic parameters of Pb^{2+} and Cu^{2+} by MnO_2/Mn_2O_3 nanoparticle.

Metal	q_e (exp) (mg g ⁻¹)	Ps-Firt-Order Kinetic			Ps-Sec-Order Kinetic		
		K_1q_e (cal)	R^2		K_2q_e (cal)	R^2	
Pb^{2+}	19.48	0.023	5.713	0.419	0.01	20.1490.971	
Cu^{2+}	24.92	0.089	2.319	0.9385	0.09	25.125	0.999

4. Conclusion

MnO_2/Mn_2O_3 nanoparticles were produced in this study using an extract from the husks of *Helianthus annuus* (sunflower) seeds. These nanoparticles were then employed as an efficient adsorbent to extract lead and Copper ions from tainted water. The adsorption capacity of the produced nanoparticles was influenced by time, pH, initial metal concentrations, and adsorbent dosage. Pb and Cd ion adsorption onto MnO_2/Mn_2O_3 -NPs was modelled using second-order rate type and Langmuir isotherms. The models' fit indicated that the adsorption mechanism was chemisorption-based and homogeneous.

The remarkable potential of these environmentally benign MnO_2/Mn_2O_3 NPs was demonstrated by the Langmuir isotherm model, which calculated the highest adsorption capacities for Pb and Cu were 26.24 mg g⁻¹ and 2000 mg g⁻¹, respectively. According to our findings, MnO_2/Mn_2O_3 nanoparticles may be a good alternative for the elimination of Cu and Pb ions with high removal efficiency in a relatively short amount of time. These nanoparticles may also be employed to eliminate other contaminants, such as polychlorinated biphenyls and organic dyes.

Acknowledgments

The authors would like to thank the Scientific and Technical Research Center in Physico-Chemical Analysis (CRAPC), University of Kasdi Merbah, Ouargla, Algeria.

References

- [1] Yang, J., et al., *Nanomaterials*, 9(3): p. 424. (2019); <https://doi.org/10.3390/nano9030424>
- [2] Reglero, M.M., et al., *Environmental pollution*, 157(4): p. 1388-1395. (2009); <https://doi.org/10.1016/j.envpol.2008.11.036>
- [3] Kampa, M. and E. Castanas, . *Environmental pollution*, 151(2): p. 362-367. (2008); <https://doi.org/10.1016/j.envpol.2007.06.012>
- [4] Cocârță, D., S. Neamțu, A. Reșetar Deac, *International Journal of Environmental Science and Technology*, 13: p. 2025-2036. (2016); <https://doi.org/10.1007/s13762-011-0009-3>
- [5] Afroze, S., T.K. Sen, *Water, Air, & Soil Pollution*, 229: p. 1-50. (2018); <https://doi.org/10.1007/s11270-018-3869-z>
- [6] Lawrence K. Wang PhD, PE, DEE, David A. Vaccari PhD, PE, DEE, Yan Li PE, MS, Nazih K. Shammas PhD, *Physicochemical Treatment Processes*. Hum. Press, Totowa, New Jersey v 3: p. 141-197. (2005).
- [7] Bodalo-Santoyo, A., et al., *Desalination*, 155(2): p. 101-108. (2003); [https://doi.org/10.1016/S0011-9164\(03\)00287-X](https://doi.org/10.1016/S0011-9164(03)00287-X)
- [8] Walsh, F.C., G.W. Reade, in *Studies in environmental science*, Elsevier. p. 3-44. (1994); [https://doi.org/10.1016/S0166-1116\(08\)70546-6](https://doi.org/10.1016/S0166-1116(08)70546-6)
- [9] Xing, Y., X. Chen, D. Wang, *Environmental science and technology*, 41(4): p. 1439-1443. (2007); <https://doi.org/10.1021/es061499l>
- [10] Ersahin, M.E., et al., *Bioresource technology*, 122: p. 196-206. (2012); <https://doi.org/10.1016/j.biortech.2012.03.086>

- [11] Zhang, P., H.H. Hahn, E. Hoffmann, *Acta hydrochimica et hydrobiologica*, 31(2): p. 145-151. (2003); <https://doi.org/10.1002/ahch.200300483>
- [12] Rykowska, I., W. Wasiak, and J. Byra, *Chemical Papers*, 62: p. 255-259. (2008); <https://doi.org/10.2478/s11696-008-0020-4>
- [13] Batley, G. and Y. Farrar, *Analytica Chimica Acta*, 99(2): p. 283-292. (1978); [https://doi.org/10.1016/S0003-2670\(01\)83569-8](https://doi.org/10.1016/S0003-2670(01)83569-8)
- [14] Srivastava, V., et al., *Journal of chemical & engineering data*, 56(4): p. 1414-1422. (2011); <https://doi.org/10.1021/je101152b>
- [15] Fu, F., Q. Wang, *Journal of environmental management*, 92(3): p. 407-418. (2011); <https://doi.org/10.1016/j.jenvman.2010.11.011>
- [16] Zamboulis, D., et al., *Journal of Chemical Technology & Biotechnology*, 86(3): p. 335-344. (2011); <https://doi.org/10.1002/jctb.2552>
- [17] Schneider, A., et al., *Journal of Chemical Technology & Biotechnology*, 97(9): p. 2305-2316. (2022); <https://doi.org/10.1002/jctb.6923>
- [18] El-Enein, S.A., et al., *Environmental Processes*, 7: p. 463-477. (2020); <https://doi.org/10.1007/s40710-020-00430-x>
- [19] Saleem, J., et al., *Biomass Conversion and Biorefinery*, 9: p. 775-802. (2019); <https://doi.org/10.1007/s13399-019-00473-7>
- [20] Tan, W.K., et al., *Nanomaterials*, 11(1): p. 181. (2021); <https://doi.org/10.3390/nano11010181>
- [21] Millot, N., et al., *The Journal of Physical Chemistry B*, 107(24): p. 5740-5750. (2003); <https://doi.org/10.1021/jp022312p>
- [22] Amsaveni, P., et al., *Journal of Physics and Chemistry of Solids*, 144: p. 109429. (2020); <https://doi.org/10.1016/j.jpcs.2020.109429>
- [23] Dessie, Y., S. Tadesse, R. Eswaramoorthy, *Arabian Journal of Chemistry*, 13(8): p. 6472-6492. (2020); <https://doi.org/10.1016/j.arabjc.2020.06.006>
- [24] Reddy, R.N., R.G. Reddy, *Journal of Power Sources*, 132(1-2): p. 315-320. (2004); <https://doi.org/10.1016/j.jpowsour.2003.12.054>
- [25] Wadhawan, S., et al., *Journal of Water Process Engineering*, 33: p. 101038. (2020); <https://doi.org/10.1016/j.jwpe.2019.101038>
- [26] Mahmoud, A.E.D., *Journal of environmental management*, 270: p. 110911; (2020). <https://doi.org/10.1016/j.jenvman.2020.110911>
- [27] Mahmoud, A.E.D., et al., *Scientific Reports*, 11(1): p. 12547 (2021); <https://doi.org/10.1038/s41598-021-91093-7>
- [28] Al-Mur, B.A., *Water*, 15(3): p. 455. (2023); <https://doi.org/10.3390/w15030455>
- [29] Dewi, N.O.M., Y. Yulizar, *Materials Today: Proceedings*, 22: p. 199-204. (2020); <https://doi.org/10.3390/w15030455>
- [30] Ho, Y.-S., G. McKay, *Process biochemistry*, 34(5): p. 451-465 (1999); [https://doi.org/10.1016/S0032-9592\(98\)00112-5](https://doi.org/10.1016/S0032-9592(98)00112-5)
- [31] Jasper, E.E., V.O. Ajibola, J.C. Onwuka, *Applied Water Science*, 10(6): p. 1-11. (2020); <https://doi.org/10.1007/s13201-020-01218-y>
- [32] Marczewski, A.W., et al., *Adsorption*, 22: p. 777-790. (2016); <https://doi.org/10.1007/s10450-016-9774-0>
- [33] Ahmad, N.H., M.A. Mohamed, S.F.M. Yusoff, *Journal of Sol-Gel Science and Technology*, 94: p. 322-334. (2020); <https://doi.org/10.1007/s10971-020-05254-7>
- [34] Langmuir, I., *Journal of the American chemical society*, 38(11): p. 2221-2295. (1916); <https://doi.org/10.1021/ja02268a002>
- [35] Freundlich, H.M.F., *J. Phys. chem.*, 57(385471): p. 1100-1107. (1906)
- [36] Haines, J., J. Léger, S. Hoyau, *Journal of Physics and Chemistry of Solids*, 56(7): p. 965-973. (1995); [https://doi.org/10.1016/0022-3697\(95\)00037-2](https://doi.org/10.1016/0022-3697(95)00037-2)
- [37] Teli, A.M., et al., *Applied Surface Science*, 511: p. 145466. (2020); <https://doi.org/10.1016/j.apsusc.2020.145466>
- [38] Barhoum, A., et al., *Crystal Growth & Design*, 15(2): p. 573-580. (2015); <https://doi.org/10.1021/cg501121t>

- [39] Manjula, R., et al., *Materials Today: Proceedings*, 26: p. 3559-3563. (2020); <https://doi.org/10.1016/j.matpr.2019.07.396>
- [40] Oliveira, R.N., et al., *Matéria (Rio de Janeiro)*, 21(03): p. 767-779 (2016); <https://doi.org/10.1590/S1517-707620160003.0072>
- [41] Hayoun, B., et al., *Applied Sciences*, 10(9): p. 3271. (2020); <https://doi.org/10.3390/app10093271>
- [42] Yusoff, N.F.M., et al., *Scientific Reports*, 10(1): p. 9207. (2020); <https://doi.org/10.1038/s41598-020-66148-w>
- [43] Parikh, S.J., J. Chorover, *Geomicrobiology Journal*, 22(5): p. 207-218.(2005); <https://doi.org/10.1080/01490450590947724>
- [44] Liu, J., et al., *Energies*, 11(3): p. 654.(2018); <https://doi.org/10.3390/en11030654>
- [45] Sharma, S., P. Chauhan, S. Husain. *Adv. Mater. Proc.*1(2),p220-225(2016); <https://doi.org/10.5185/amp.2016/220>
- [46] Pinaud, B.A., et al., *The Journal of Physical Chemistry C*, 115(23): p. 11830-11838. (2011); <https://doi.org/10.1021/jp200015p>
- [47] Chen, X., et al., *Marine drugs*, 16(8): p. 277. (2018); <https://doi.org/10.3390/md16080277>
- [48] Hosain, A.N., et al., *Journal of Environmental Chemical Engineering*, 8(5): p. 104316. (2020); <https://doi.org/10.1016/j.jece.2020.104316>
- [49] Jeon, C., W.H. Höll, *Water Research*, 37(19): p. 4770-4780. (2003); [https://doi.org/10.1016/S0043-1354\(03\)00431-7](https://doi.org/10.1016/S0043-1354(03)00431-7)
- [50] Khulbe, K., T. Matsuura, *Applied Water Science*, 8: p. 1-30. (2018); <https://doi.org/10.1007/s13201-018-0661-6>
- [51] Semerjian, L., *Environmental technology & innovation*, 12: p. 91-103, (2018); <https://doi.org/10.1016/j.eti.2018.08.005>
- [52] Keochaiyom, B., et al., *Journal of colloid and interface science*, 505: p. 824-835. (2017); <https://doi.org/10.1016/j.jcis.2017.06.056>
- [53] Dubey, R., J. Bajpai, A. Bajpai, *Environmental Nanotechnology, Monitoring & Management*, 6: p. 32-44. (2016); <https://doi.org/10.1016/j.enmm.2016.06.008>
- [54] Kundu, S., A.K. Gupta, *Chemical Engineering Journal*, 122(1-2): p. 93-106. (2006); <https://doi.org/10.1016/j.cej.2006.06.002>
- [55] Kabiri, S., et al., *ACS applied materials & interfaces*, 7(22): p. 11815-11823. (2015); <https://doi.org/10.1021/acsami.5b01159>